Watershed Controls and Tropical Cyclone-Induced Changes in River Hydraulic Geometry in Puerto Rico

Yihan Li[a,*], Daniel B. Wright[a], Brian P. Bledsoe[b]

[a] University of Wisconsin-Madison, 1415 Engineering Dr, Madison, Wisconsin 53706, United States of America

[b] University of Georgia, 200 D.W. Brooks Dr, Athens, Georgia 30602, United States of America

[*] Corresponding Author. E-mail address: yihan.li@wisc.edu (Y. Li).

Abstract

At-a-station hydraulic geometry (AHG), which describes how channel width, depth, and velocity vary with discharge at a river cross section, has long been used to study fluvial processes. For example, identification of landscape and river reach drivers of hydraulic geometry can help to predict channel properties at ungaged sites and to understand channel responses to major floods. Most prior AHG studies have focused on mid-latitude, temperate regions. Tropical zones—including those affected by tropical cyclones (TCs)—have received less attention. This study analyzed spatial and temporal variability in hydraulic geometry at 24 stream gaging sites in Puerto Rico, and identified the watershed and river reach characteristics that correlate with each hydraulic geometry parameter. These characteristics were then used to build regression models of AHG parameters, with relatively high predictive power. The largest flood events from each site were found to cause systematic changes to AHG parameters; most of these floods were caused by major TCs. Upstream drainage area, average watershed elevation, watershed land cover and other characteristics were found to be significant predictors of AHG parameters. Reaches with steeper slopes were found to have limited lateral adjustability, which may reflect consolidated bank materials and valley confinement. Watersheds with high percentages of forested area showed greater changes in roughness but less vertical adjustability than more developed watersheds. These correlation results help inform whether river channel properties in Puerto Rico and similar environments are resistant to the forces of TC-induced flooding, and how these properties are affected by major floods.

Keywords:

Hydraulic Geometry; Tropical Cyclone; Flood Hazard; Puerto Rico; Land Use

Acronyms Definition:

- AHG: At-a-station hydraulic geometry
- TC: Tropical Cyclone
- USGS: U.S. Geological Survey
- NWIS: National Water Information System
- NOAA: National Oceanic and Atmospheric Administration
- NLS: Non-linear squares
- WHR: median width to depth ratio
- NACW: normalized active channel width
- RMSE: root mean square error
- rRMSE: relative root mean square error

1. Introduction

River cross sectional geometry is both a determinant and result of fluvial processes, including flood conveyance (Guan et al., 2016; Kale & Hire, 2004), sediment transport (Bennet & Bridge, 1995; Bridge, 1993), riparian vegetation growth (Malkinson & Wittenberg, 2007) and channel erosion (Millar & Quick, 1993; Wiman & Almstedt, 1997). At-a-station hydraulic geometry (AHG) describes the relationships between discharge vs. water-surface width, mean depth, and mean velocity at individual river cross sections. Power law formulations have long been used to model AHG, and these formulations have been widely applied to understand river geomorphology (e.g. Andreadis et al., 2013; Barefoot et al., 2019; Knighton & Wharton, 2014; Leopold et al., 1964; Reid et al., 2010; Stewardson, 2005). The standard AHG formulation, which first appeared in Leopold & Maddock (1953), is

$$w = aQ^b \quad \text{Eqn. 1}$$

$$d = cQ^f \quad \text{Eqn. 2}$$

$$v = kQ^m \quad \text{Eqn. 3}$$

where w is channel width (typically the wetted width), d is the hydraulic depth (i.e. cross-sectional area divided by w), v is mean stream velocity, and Q is the instantaneous discharge. The requirement of continuity,

$$Q = wdv = ackQ^{b+f+m} \quad \text{Eqn.4}$$

implies the constraints $ack = 1$ and $b + f + m = 1$.

The coefficients (a, c, and k) describe the relative magnitude of channel width, channel depth and velocity (or roughness), while the exponents (b, f, and m) provide insight into how channel width, channel depth and velocity change with discharge. Notwithstanding these constraints, the coefficients and exponents from Eqns. 1-4 can vary substantially from place to place (Morel et al., 2020b; Park, 1977), and researchers have yet to fully reveal the physical principles that underly AHG behavior (Jia et al., 2017; Morel et al., 2019; not for lack of trying, e.g. Dingman, 2007; Ferguson, 1986). Watershed and river reach characteristics that have been shown to explain some observed AHG variability include drainage area (Qin et al., 2020), watershed orientation and

channel substrate (Turowski et al., 2008), suspended sediment load (Wang et al., 2006), and reach slope (David et al., 2010). While recent work has built predictive models for AHG exponents (*b*, *f*, and *m*; Morel et al., 2019, 2020a), the coefficients *a*, *c*, and *k* have received less attention (Morel et al., 2020a; Qin et al., 2020; Ran et al., 2012; Turowski et al., 2008). Relationships have also been shown between AHG parameters from various cross sections within individual river systems (Barber & Gleason, 2018; Brinkerhoff et al., 2019; Dingman, 2007; Gleason, 2015; Gleason & Smith, 2014; Turowski et al., 2008).

Channel morphology has also been shown to change over time due to natural processes like changes in suspended sediment load (Wang et al., 2006), changing high latitude river ice regimes (Best et al., 2005), floods (e.g. Hajdukiewicz et al., 2016; Magilligan et al., 2015; Sholtes et al., 2018; Yochum et al., 2017), and due to human activities including urbanization (e.g. Booth, 1990; Hawley et al., 2013) land cover changes (Fitzpatrick & Knox, 2000), reservoir operations (Ran et al., 2012; Su et al., 2015), and sand excavation (Zhang et al., 2015). Nonetheless, analyses of temporal changes in AHG and its causes remain relatively rare (Qin et al., 2020), and most existing studies are confined to the mid-latitudes, while data limitations mean that AHG in more tropical zones—with their unique hydroclimatic and geologic conditions—have been less studied (see Lewis, 1969, Phillips & Scatena, 2013, and Turowski et al., 2008 for exceptions).

Tropical cyclones (TCs) hit Puerto Rico (PR) frequently and are often associated with heavy and intense rainfall. This rainfall, combined with the steep mountainous terrain in PR and similar environments, can produce some of the largest flood peaks per unit watershed area in the world (Ogden, 2016; Smith et al., 2005). These floods can cause landslides, debris flows, mass wasting, and fluvial erosion, which redistribute large amounts of sediment along the river (West et al., 2011) and are capable of causing systematic lateral and vertical channel adjustments (e.g. Yousefi et al., 2018). Li et al. (2020) found that channel conveyance capacity can change substantially as a result of TC flooding. That study did not, however, examine how these changes manifest in terms of channel geometric properties, and failed to isolate upstream watershed characteristics or local river reach influence (e.g., slope, land cover) that could explain the observed conveyance capacity evolution.

This study attempts to connect the findings of Li et al. (2020) with the AHG framework by examining the watershed and river reach determinants of AHG—including whether or not it is

feasible to estimate AHG at ungaged sites—and also by evaluating the potential for AHG response to major flood events, which are almost always caused by TCs in Puerto Rico. Such findings could be valuable for applications such as simplified discharge estimation (Huang et al., 2018; Wang et al., 2019): with a suitable AHG relationship between width and discharge, one can obtain reasonably accurate estimates of discharge based on channel widths measured from *in-situ* or remotely-sensed imagery. Identification of relevant watershed and river reach characteristics and subsequent transferal to ungaged sites, meanwhile, could be used to inform flood risk management, river restoration, and related actions.

This study examined AHG parameters for 24 sites in PR. Correlation analyses were used to identify the watershed and river reach characteristics that are potentially predictive of AHG parameter estimates. These characteristics were used to build multiple linear regression models for each parameter, with cross validation used to evaluate their applicability to ungaged sites. Channel geometry responses to TC floods were examined by calculating changes in AHG parameters after major storms and comparing changes to watershed and river reach characteristics. The study region and data used in this study are described in Section 2. The methodology is described in Section 3. Results follow in Section 4, while discussion and conclusions are provided in Sections 5 and 6, respectively.

2. Study Region and Data

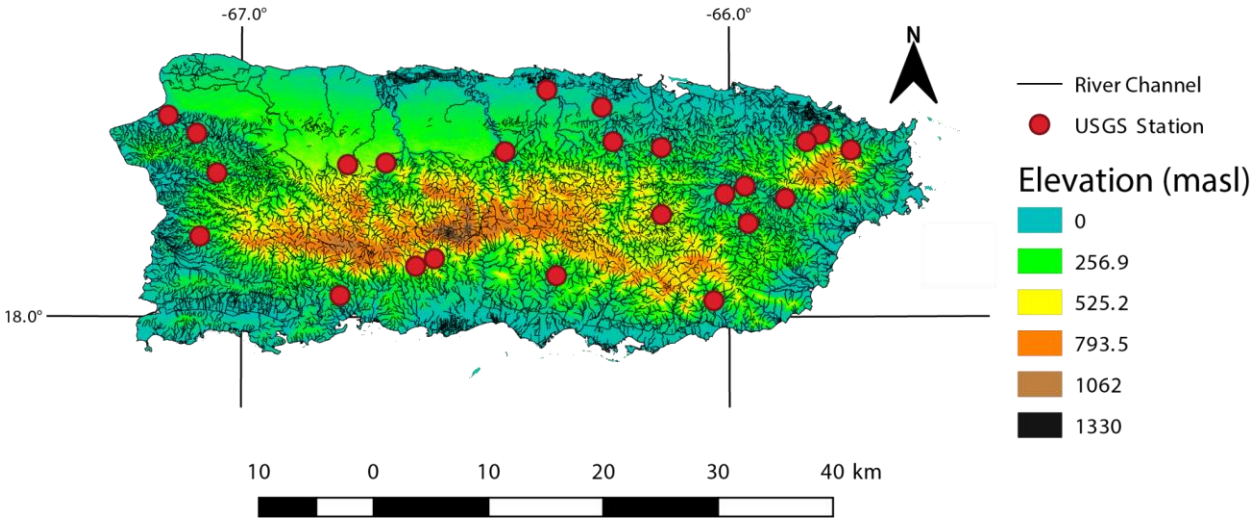

Fig. 1: Map of Puerto Rico, showing the USGS stream gages considered in this study and elevation in meters above sea level (masl; from OCM Partners, 2019). River networks (U.S. Geological Survey, 2006) are shown in thin black lines.

Puerto Rico (PR) is a mountainous island located in the northeast Caribbean. The average elevation of the mountainous middle part exceeds 1300 m above sea level (masl), while the average elevation of the less steep margin is about 500 masl. Annual precipitation ranges from around 500 cm for the mountainous center to 100-400 cm in the coastal lowlands (Daly et al., 2003). A monsoon season begins in May and usually lasts until October, overlapping with the June-November North Atlantic TC season. Limited by the island's aspect and east-west mountain range, its rivers generally range from <10 kilometers to about 50 kilometers in length, with the longest—Rio de la Plata—measuring 74 kilometers, and from <10 meters to more than 60 meters in width.

Our AHG estimation relied on field measurements of channel geometry and velocity, which the US Geological Survey (USGS) performs at stream gage sites on a fairly regular basis (roughly monthly) to maintain accurate rating curves, which are then used for continuous discharge estimation (U.S. Geological Survey, 2021b). These field measurements were obtained from the National Water Information System (NWIS) maintained by the USGS. Annual instantaneous peak discharges (U.S. Geological Survey, 2021a) were used to identify the date with the largest flood in each site's record.

We applied rigorous screening to identify suitable USGS stream gage stations. Sites with recorded flags indicating influence by nearby dams, as well as those located in the vicinity of man-made structures such as weirs were excluded due to their influence on AHG (Reisenbüchler et al., 2019). Field measurement records in PR available through NWIS usually start around 1990, though several sites' records date back to the early 1980s. If a station is reported to have experienced datum changes, we avoided all observations before the most recent datum change. The site was excluded from the analysis if the most recent datum change occurred later than 1990. We applied the data accuracy criteria of Slater et al. (2015), who only considered field measurements in which the discharge is within one percent of the product of channel velocity and cross-sectional channel area, as reported by the USGS, and those made in close proximity to the gage station (within 300 feet [91 m]; hardly any field measurements were made directly at the gaged cross section). Only sites that have continuous daily discharge records in the same period of the field measurements

were included. 24 sites satisfied these criteria (Fig. 1; Table S1). The limited number of sites in the northwestern portion of the island is linked to the lower drainage density there.

Upstream watershed and river reach characteristics were obtained or estimated from public GIS and remote sensing resources and used to calculate correlations with and to predict AHG parameters. Watershed boundaries, along with the upstream drainage area, corresponding to each stream gage were downloaded from NWIS. Watershed-averaged elevation and slope were calculated for each gage based on a digital elevation model from the National Oceanic and Atmospheric Administration (NOAA) National Centers for Environmental Information. We matched the reach segment from the river network (U.S. Geological Survey, 2006) to each of the 24 gauging sites, and then measured the reach slope and sinuosity of the reach. Reach widths were estimated via remote sensing imagery available through the Google Earth application. Percentages of developed, forested, and planted (agricultural) areas were obtained from the USGS GAGES-II dataset (Falcone, 2011). (Note that land use metrics are "static," i.e., only available at the time point when GAGES-II data were taken in 2011.)

3. Methodology

3.1 Hydraulic Geometry Parameter Estimation

To study spatial variation of the hydraulic geometry, we fit models to the entire period of field measurements to get parameter estimates for each site (see black lines in Fig. 2 for examples). The parameter values in Eqns. 1-3 were estimated via the nonlinear least squares (NLS) regression function in the R programming language (R core team, 2020). The residuals of each NLS regression model were examined for homoscedasticity, independence and normality using the package "nlstools" (e.g. Fig. S1). Units used in this study are m^3/s for discharge, m for depth and width, and m/s for velocity; the resulting units for a, c, and k are s/m^2, s/m^2 and m^{-3}, respectively Channel surface water widths and mean velocities were used to fit channel Eqns. 1 and 3, respectively, while hydraulic mean depths in Eqn. 2 were calculated by dividing flow areas by surface water widths (after Barber & Gleason, 2018; Brinkerhoff et al., 2019; Doll et al., 2002; Shen et al., 2016).

The fitted parameters obtained via NLS did not strictly satisfy continuity (Eqn. 4), though nearly so (results not shown). We thus applied a normalization used in prior studies (Jowett, 1998; Lee et al., 2019; Park, 1977) to enforce continuity (Eqn. 5 and 6):

$a_{adjusted} = \frac{a_{fitted}}{(a_{fitted} c_{fitted} k_{fitted})^{\frac{1}{3}}}$, similar for c and k Eqn. 5

$b_{adjusted} = \frac{b_{fitted}}{b_{fitted} + f_{fitted} + m_{fitted}}$, similar for f and m Eqn. 6.

We also reproduced all subsequent analyses without this normalization. Results with and without normalization were nearly equivalent; results without normalization are omitted for brevity.

Eqns. 1 and 2 imply that channel cross-sectional geometry can be described by an equation of the form

$d = \frac{c}{a^{\frac{f}{b}}} w^{\frac{f}{b}}$ Eqn. 7

Eqn. 7 shows that depth is proportional to the surface water width to the power of $\frac{f}{b}$. Prior studies have examined the value of $\frac{f}{b}$ as an indicator of channel cross sectional shape (Ferguson, 1986; Qin et al., 2020; Turowski et al., 2008). For example, width is proportional to depth when $\frac{f}{b}$=1, implying a triangular cross section while $\frac{f}{b}$=2 implies a parabolic form. When $b = 0$, $\frac{f}{b}$ would be infinity, implying that the wetted width does not increase with discharge, as in cases of rectangular cross section. $\frac{f}{b}$<1 represents a convex upwards curved channel section indicative of a cut bank/point bar form with width increasing more than depth for medium-to-high discharges (See Fig.3 in Ferguson, 1986). The ratio $\frac{c}{a^{\frac{f}{b}}}$, which indicates relative bank steepness for a particular value of $\frac{f}{b}$, is absent from earlier studies. We calculated $\frac{f}{b}$ and $\frac{c}{a^{\frac{f}{b}}}$ from our AHG estimates and refer to them as “bank shape parameters.”

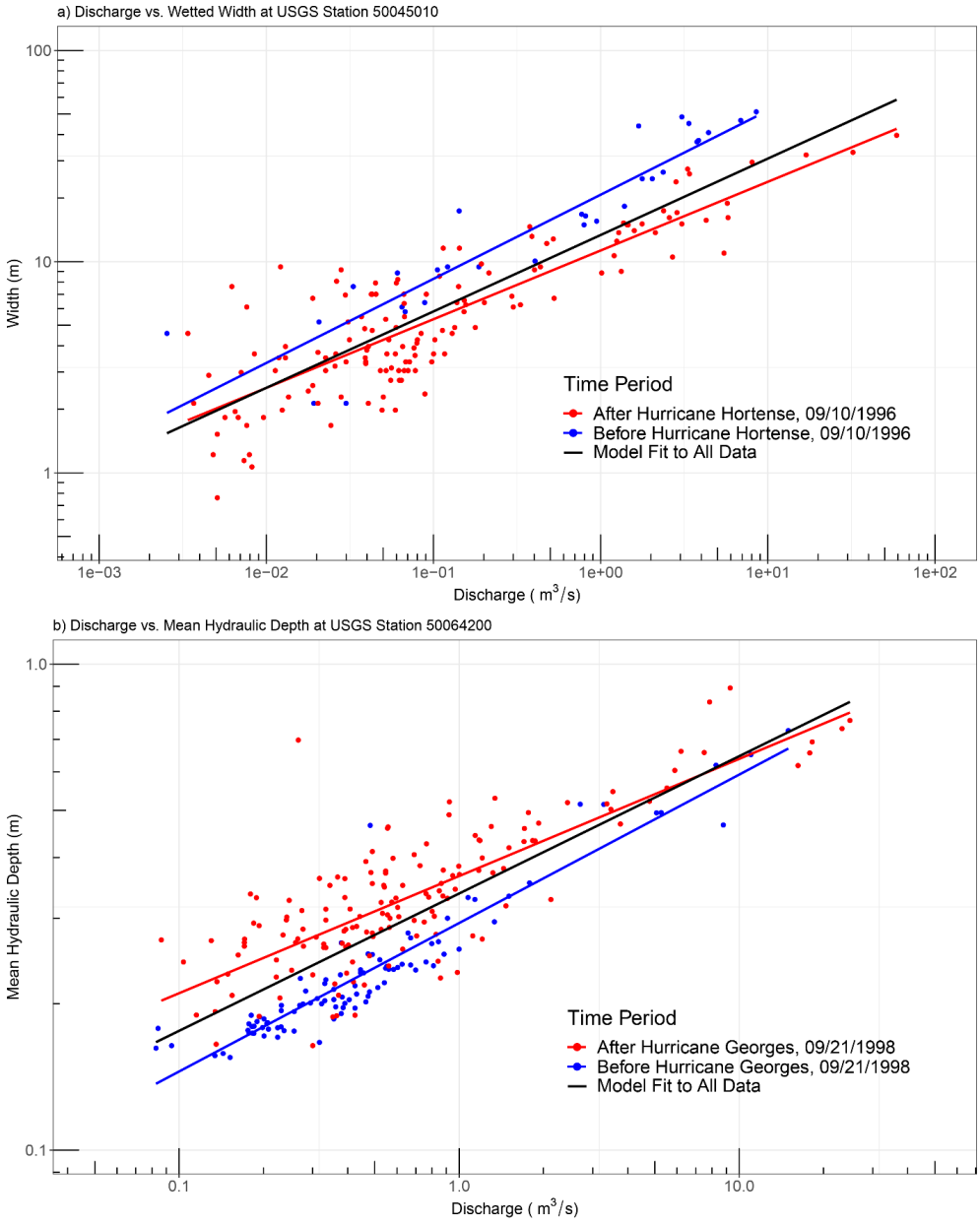

Fig. 2 a) Discharge vs. width at site 50045010. The black line represents the fitted nonlinear least squares model using all data available at the site since 1992. The blue and red lines correspond to the model fit only to the field measurements before and after Hurricane Hortense, respectively. b) Discharge over mean depth at site 50064200. The black line represents the nonlinear least squares

model using all data available at the site since 1990. The blue and red lines correspond to the model fit only to the field measurements before and after Hurricane Georges, respectively.

3.2 Watershed and River Reach Characteristics and Correlation Analyses

Upstream watershed and reach-scale characteristics were estimated to examine their relationships to AHG and AHG parameter responses to floods. Other than the characteristics introduced in the data section, we included three additional variables following Morel et al., (2019): Froude number at median discharge of all available field measurements for each site(Fr_{50}), the median width to depth ratio (*WHR*), and normalized active channel width (*NACW*). These are calculated as

$$Fr_{50} = \frac{Q_{50}}{g^{0.5} H_{50}^{1.5} W_{50}} \quad \text{Eqn. 8}$$

$$WHR = \frac{W_{50}}{H_{50}} \quad \text{Eqn. 9}$$

$$NACW = \frac{channel\ width}{(watershed\ area)^{0.42}} \quad \text{Eqn. 10,}$$

where Q_{50}, W_{50} and H_{50} are median discharge, median flow wetted width, and median depth, respectively. Finally, the normalized two-year flood (calculated as the median of annual instantaneous peak flows from NWIS divided by the upstream drainage area) was included to describe the "peakiness" of a watershed's flood regime. Kendall's tau nonparametric rank correlation (Kendall, 1938) was used to identify relationships between watershed/reach characteristics and AHG parameters.

3.3 AHG predictive regression models

We used a stepwise process to develop models to predict AHG parameters based on watershed and river reach characteristics. We began by creating multiple linear regression models for each AHG parameter based on all available predictors. These were reduced to final predictive models via trial and error. In order to balance model predictive power and complexity, final models were those with the highest adjusted R-squared values. Some significant variables were not used in the models due to collinearity among predictors. Following Morel et al. (2019), we took the natural log and the square root of elevation and watershed area, respectively, before considering them as predictors.

To evaluate the potential predictive power of the final regression models at similar ungaged sites in Puerto Rico, as well as to avoid overfitting, we performed leave-one-out cross-validation to estimate the root mean square error of the predicted values of each parameter. Keeping the predictors fixed, we removed one site and retrained each model with data from the other 23 locations. We then used the trained model to predict the parameter values for the withheld site. We repeated this for all sites and then compared the predicted parameters with the observed parameter values from former steps.

3.4 AHG Temporal Variation Due to Tropical Cyclones

Li et al. (2020) showed that recent major TCs, primarily Hurricanes Hortense (1996), Georges (1998), and Maria (2017), caused substantial changes in river channel conveyance capacity in PR. This earlier work, however, did little to elucidate more specific geomorphic changes. AHG parameters can indeed change substantially in response to TCs (see the red and blue lines in Fig. 2, which show distinct AHG relationships estimated before and after major storms). We identified the largest "local" flood event—the largest annual peak streamflow value for each site—to separate the field measurements into two time series, before and after this largest local flood event. Hurricanes Hortense and Georges caused the largest flood events at six sites each, while Hurricane Maria caused the largest flood at ten others. The largest floods at the two remaining sites were caused by non-TC storms. We again followed the methodology in Section 3.1 to estimate AHG parameters (see Section 4.3) but only for periods four years before and four years after these identified flood events. We calculated "before-and-after" percentage changes in AHG parameters (including bank shape parameters) by subtracting the values after the largest flood event from the values before, and dividing the difference by the latter value. These changes were then tested for correlation with watershed and river reach characteristics using the nonparametric rank correlation mentioned in Sec. 3.2. We extracted the peak discharges of the local largest flood events, and divided them by the discharges of the 2-year flood at the same site to get normalized discharges of the largest local flood events. These normalized flood discharges were included as an additional characteristic in the correlation analysis specific to AHG parameter changes caused by floods.

4. Results

4.1 AHG Parameter Estimates and Correlation Tests

The power models fit reasonably well (p-values much less than 0.05) to all six parameters at all sites except for velocity at site 50064200, which yielded a p-value of 0.056 (Table S2). The average values for the exponents were 0.230, 0.394, and 0.376 for b, f and m, respectively. A ternary plot (Fig. 3a) shows similar distributions of exponents from this study and from the earlier AHG studies in Puerto Rico of Lewis (1969) and Phillips & Scatena (2013). The results are also similar to those from Leopold & Maddock (1953) in the mainland midwestern United States and Leopold & Miller (1956) in mainland ephemeral rivers (results not shown). Similarly to Phillips & Scatena (2013) observations, we found that the width exponent is usually less than 0.33, with only one exception where $b = 0.344$.

The relationships between AHG parameter estimates and the various watershed and reach characteristics are tabulated in terms of Kendall's tau correlation (Table 1), while those of most obvious interest are shown in additional ternary plots (Fig. 3b-d). Upstream watershed area was found to be significantly positively (negatively) correlated with $f(m)$, while the opposite was found for both percentage of developed area and planted area. Average upstream watershed elevation, slope, and the percentage of forested area were found to be significant and negatively (positively) correlated with f (m). No characteristics were found to be significantly associated with b, and no other characteristics were found to be significantly correlated with any exponents. Upstream watershed area, average watershed elevation, average reach width, average reach slope, WHR, Fr_{50}, and NACW were also found to be significantly correlated with some coefficients (Table 1). The channel shape parameters $\frac{f}{b}$ and $\frac{a}{c^{\frac{f}{b}}}$ are positively and negatively correlated (at the 5% level), respectively, with average watershed elevation. Upstream watershed area is also found to be negatively correlated with $\frac{a}{c^{\frac{f}{b}}}$, while average upstream watershed slope is found to be negatively correlated with $\frac{f}{b}$, both of which are significant at the 5% level.

Table 1. Kendall's tau correlation results with p-values shown in parentheses. Relationships significant at the 5% level are bolded.

Watershed and River Reach Characteristics	a	c	k	b	f	m	$\frac{f}{b}$	$\frac{c}{a^{\frac{f}{b}}}$
Normalized Two Year Flood ($\frac{m^3}{s}/km^2$)	-0.043 (0.79)	0.27 (0.07)	-0.2 (0.17)	0.17 (0.27)	-0.1 (0.51)	0.036 (0.83)	-0.14 (0.36)	0.11 (0.48)
Watershed Area (km^2)	**0.48 (<0.001)**	**-0.5 (<0.001)**	-0.062 (0.67)	-0.018 (0.9)	**0.36 (0.014)**	**-0.36 (0.014)**	0.19 (0.19)	**-0.38 (0.009)**
Reach width (m)	**0.42 (0.004)**	-0.17 (0.27)	**-0.36 (0.013)**	0.21 (0.16)	0.2 (0.17)	-0.25 (0.087)	0.051 (0.75)	-0.18 (0.23)
Reach slope (m/m)	**-0.33 (0.023)**	0.11 (0.48)	0.19 (0.21)	-0.065 (0.68)	-0.17 (0.25)	0.17 (0.27)	-0.11 (0.48)	0.22 (0.13)
Watershed Forested Area (%)	-0.029 (0.86)	0.27 (0.07)	-0.25 (0.097)	-0.094 (0.54)	**-0.3 (0.039)**	**0.38 (0.008)**	-0.094 (0.54)	0.094 (0.54)
Watershed Developed Area (%)	0.08 (0.61)	-0.23 (0.12)	0.25 (0.087)	0.087 (0.57)	**0.51 (<0.001)**	**-0.51 (<0.001)**	0.22 (0.14)	-0.19 (0.21)
Watershed Planted Area (%)	0.11 (0.47)	-0.13 (0.39)	0.093 (0.54)	0.07 (0.65)	**0.49 (0.001)**	**-0.44 (0.004)**	0.26 (0.092)	-0.23 (0.14)
Average watershed slope	-0.072 (0.64)	0.15 (0.31)	-0.23 (0.12)	0.007 (0.98)	**-0.57 (<0.001)**	**0.54 (<0.001)**	**-0.31 (0.034)**	0.22 (0.13)
Average watershed elevation (masl)	-0.17 (0.25)	**0.3 (0.044)**	-0.22 (0.14)	0.15 (0.31)	**-0.49 (<0.001)**	**0.41 (0.004)**	**-0.36 (0.015)**	**0.41 (0.004)**
WHR	0.2 (0.17)	**-0.33 (0.026)**	-0.13 (0.39)	-0.2 (0.19)	-0.26 (0.078)	0.27 (0.07)	-0.094 (0.54)	-0.094 (0.54)
Fr_{50}	0.21 (0.16)	**-0.39 (0.007)**	0.12 (0.42)	0.087 (0.57)	0.21 (0.16)	-0.28 (0.062)	-0.043 (0.79)	-0.058 (0.71)
NACW (m)	0.16 (0.29)	0.065 (0.68)	**-0.38 (0.010)**	0.27 (0.07)	-0.043 (0.79)	-0.065 (0.68)	-0.14 (0.36)	0.065 (0.68)
Sinuosity (m/m)	0.094 (0.54)	0 (1)	0.022 (0.9)	-0.058 (0.71)	0.065 (0.68)	-0.014 (0.94)	0.043 (0.79)	-0.014 (0.94)

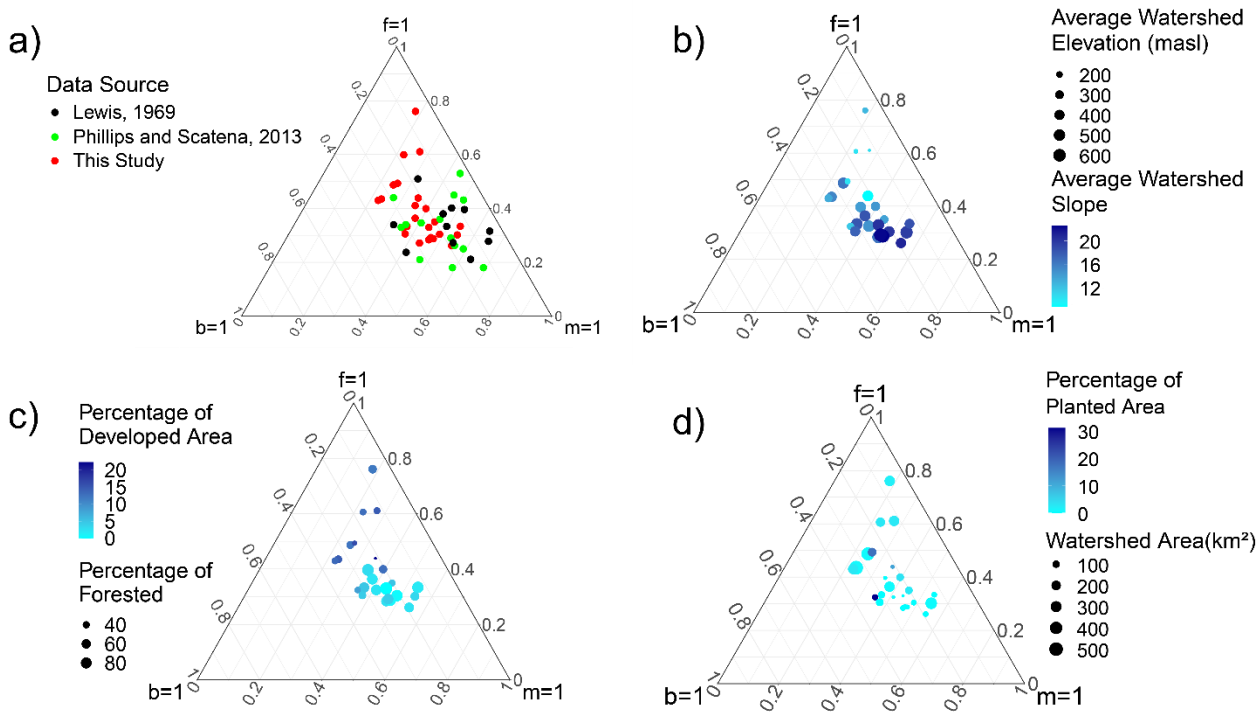

Fig. 3: Ternary plots showing the estimated exponents for the entire study period: a) Comparison to former studies in Puerto Rico, b) relationships with average watershed slope and elevation, c) relationships with percentages of developed and forested area, and d) relationships with percentage of planted area and watershed area.

The ratio $\frac{f}{b}$ was found to be negatively correlated (p=0.023) with average watershed elevation, indicating that higher-elevation rivers in PR tend toward more triangular and less rectangular channel cross-sectional shapes. Turowski et al. (2008) found a strong log-log relationship between the bank shape parameter $\frac{f}{b}$ and the exponent b for average parameter values in different studies. By comparing our data with prior studies, we found that this relationship appears to hold across a wide range of studies and study locations. The range of coefficients of the models fit separately to each of the five studies shown on this plot is 0.15 - 0.33. The range of exponents is -1.42 - -1.01. The coefficient and exponent of the model fit to our data are 0.22 and -1.35, respectively, which are within the range. The model fit range also contains the equation in Turowski et al. (2008; Fig. 4, gray line; $\frac{f}{b} = (0.28 \pm 0.06)b^{-1.12\pm0.07}$). This confirms that in Puerto Rico, as in other locations, general, steep-banked channels lead to smaller exponent b, which is indicative of width being less

adjustable, which can be caused by consolidated bank materials like cohesive soils that are common in cases of steep banks.

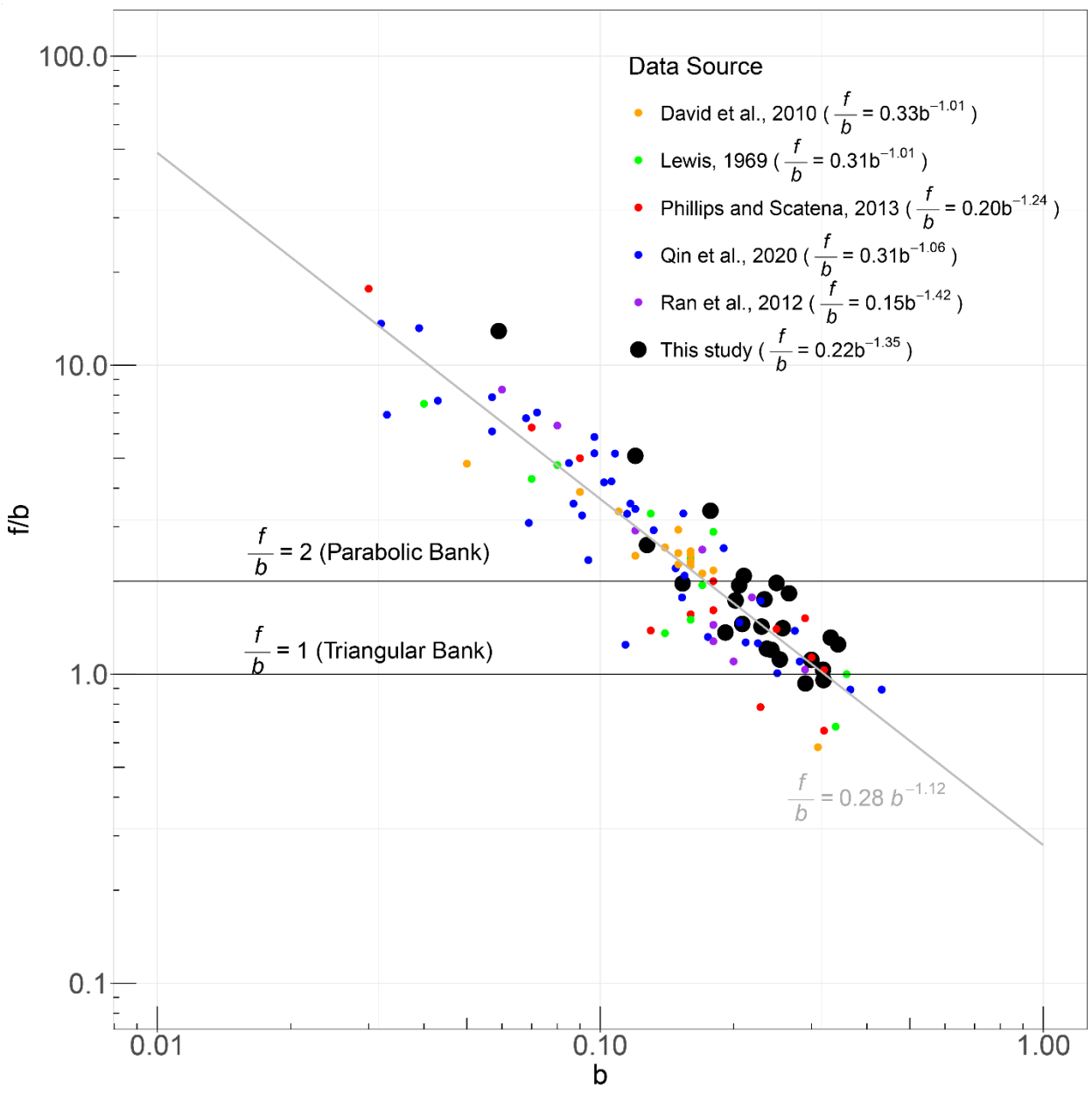

Fig. 4 Scatterplot of f/b vs. b using data from multiple former studies and this study. All model fits are significant (p-values < 10^{-3}) Gray line shows the model fit by Turowski et al. (2008), to multiple studies. The model from Turowski et al. (2008) was fit to average values of each study, rather than whole data sets from the studies. The only common study between the five former studies shown on this plot and the studies analyzed in Turowski et al. (2008) is Lewis (1969).

4.2 AHG Predictive Models

The final regression models to predict AHG parameters (Section 3.3) are shown in Table 2, along with R-squared values and overall model p-values. Among the three coefficients (exponents), $k(b)$ is least well predicted, in terms of adjusted R-squared. The regression model for b is the only model that is insignificant at 5% level. When subject to leave-one-out cross validation, all regression-based models can predict parameter values with relative root mean square error (rRMSE; RMSE divided by the average parameter value) between 10% and 30%, except for the model for b, which results in 31.2%.

Table 2. Regression-based predictive models for AHG parameters. Predictors are: width to depth ratio at median discharge (WHR), average watershed slope (S_{ws}), average watershed elevation ($Elev_{ws}$), watershed area (A_{ws}), the percentages of developed area ($Developed$), forested area ($Forested$) and planted area ($Planted$), normalized two year flood (Q_{2yr}), reach slope (S_r), reach sinuosity ($sinuosity$), channel width (w_c), normalized active channel width ($NACW$) and Froude number at median discharge (Fr_{50}). In the leave-one-out validation, models were repeatedly fit to 23 sites, and then used to predict the remaining site's parameter. RMSEs were calculated between the leave-one-out predictions estimated values shown in Table S2; units match those of the corresponding AHG parameter. Relative RMSEs were calculated by normalizing RMSEs by the mean parameter value from Table S2 and multiplying by 100.

Model Structure	Adjusted R^2	R^2	p-value	Leave-one-out RMSE (Relative RMSE)
$a = -1.97 + 0.11WHR + 0.53\sqrt{A_{ws}} + 0.066Forested$	0.83	0.85	<0.001	3.3 (25.7%)
$c = -0.36 + 0.10log\ (Elev_{ws}) + 0.0039Planted + 0.0074Q_{2yr}$	0.55	0.61	<0.001	0.048 (18.3%)
$k = 0.66 - 0.010S_{ws} - 0.039NACW - 0.0039\sqrt{A_{ws}}$	0.38	0.46	0.007	0.095 (28.2%)
$b = -0.20 - 7.6e-04WHR + 0.095log\ (Elev_{ws}) - 0.0015Forested$	0.18	0.29	0.08	0.072 (31.2%)
$f = 1.18 + 0.0033Forested + 0.015Developed - 0.18log\ (Elev_{ws})$	0.67	0.71	<0.001	0.073 (18.5%)
$m = 0.22 + 0.013S_{ws} - 0.010\sqrt{A_{ws}} + 0.0013WHR$	0.76	0.79	<0.001	0.060 (15.9%)

4.3 Hydraulic Geometry Response to Tropical Cyclones

We re-estimated AHG parameters for each site using two periods: four years before and after the largest local flood event (i.e., the highest single instantaneous flood peak for each site, see Sec.3.4). Both the percent differences between the "before-and-after" parameter values and the absolute value of these differences were calculated. The absolute values are generally indicative of the overall tendency of a site's AHG relations to change in response to a major flood, while the real difference provides the direction of that change. The differences in the parameter values of the largest local flood event are shown in Fig. 5. Percent changes in parameter values are evident at most sites and for all parameters. The changes in the depth exponent f tend to be positive in the northeastern part of the island and negative in western Puerto Rico. No obvious spatial patterns were evident for other parameters.

We then computed correlations between these parameter value changes and the various watershed and river reach characteristics (Table 3). Froude number, sinuosity, and NACW are positively and significantly (at 5% level) correlated with the real percent difference of a, while NACW is also negatively correlated (p=0.034) with the real percent difference in k. Normalized two-year flood and WHR are positively correlated with the shape coefficient $\frac{c}{a^{\frac{f}{b}}}$ (p-values are 0.042 and 0.03, respectively). The percentage of forested (developed) area is negatively (positively) correlated with the absolute percent difference of k, with p-values of 0.03 (0.008). The percentage of forested (developed) area is also positively (negatively) correlated with the absolute percent difference of b, with p-values of 0.003 (0.009) . Watershed area, reach width, and the percentage of planted area are also significantly negatively correlated with the absolute percent difference of b. The percentage of planted area (average watershed slope) is positively (negatively) correlated with the absolute percent change of c, with p=0.036 (p=0.017).

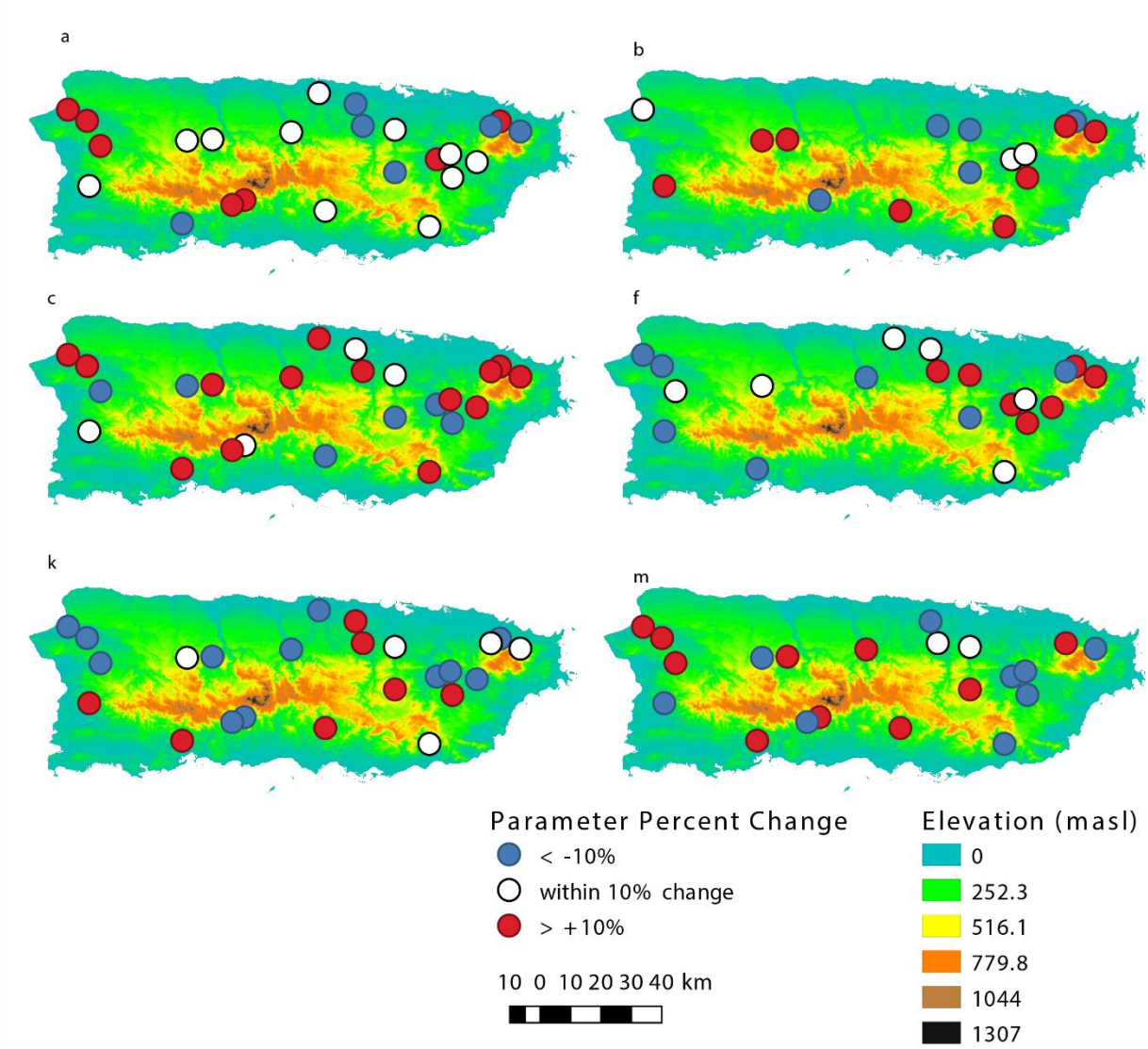

Fig. 5. Real percent parameter value changes of the largest flood event for all AHG parameters. Only the sites with significant model estimates for both before and after the largest flood event are shown on each panel. Number of sites shown on each panel: 24 for coefficients (a, c and k), 16 for b, 20 for f, and 21 for m. Blue dots are the sites with real parameter value decreases greater than 10%, while red dots are the sites with real parameter value increases greater than 10%. White dots are the sites within between 10% decreases and 10% increases.

Table 3. Kendall's Tau correlation test results of percent parameter changes caused by the largest local flood event and watershed/river reach characteristics. The values outside of the brackets are the correlations entry between the predictor and the percent parameter change, while the values

inside brackets are the correlations between the predictor and the absolute value of the percent parameter change. Quantities inside parentheses are corresponding p-values; bolded results are significant at the 5% level.

Watershed and River Reach Characteristics	a (N=24)	c (N=24)	k (N=24)	b (N=16)	f (N=20)	m (N=21)	$\frac{f}{b}$ (N=13)	$\frac{c}{a^{\frac{f}{b}}}$ (N=13)
Normalized Two Year Flood ($\frac{m^3}{s}/km^2$)	0.16 (0.29) |0.16 (0.29)|	0.17 (0.25) |0.087 (0.57)|	-0.27 (0.07) |-0.087 (0.57)|	0.23 (0.23) |0.083 (0.69)|	0.032 (0.87) |-0.063 (0.72)|	-0.17 (0.29) |-0.24 (0.14)|	-0.18 (0.44) |-0.23 (0.31)|	**0.44 (0.042)** |0.15 (0.51)|
Watershed Area (km^2)	0.083 (0.57) |-0.098 (0.5)|	-0.025 (0.86) |0.12 (0.41)|	0.0036 (0.98) |0.19 (0.21)|	-0.21 (0.26) |**-0.49 (0.0078)**|	0.1 (0.54) |0.037 (0.82)|	0.072 (0.65) |0.11 (0.49)|	0.25 (0.25) |-0.09 (0.67)|	-0.37 (0.076) |-0.039 (0.85)|
Reach width (m)	0.28 (0.062) |0.072 (0.64)|	0.13 (0.39) |0.22 (0.14)|	-0.25 (0.087) |0.087 (0.57)|	-0.22 (0.27) |**-0.4 (0.033)**|	0.22 (0.19) |0.021 (0.92)|	-0.038 (0.83) |-0.029 (0.88)|	0.31 (0.16) |-0.15 (0.51)|	-0.26 (0.25) |0.23 (0.31)|
Reach slope (m/m)	-0.043 (0.79) |0.029 (0.86)|	0 (1) | -0.13 (0.39)|	-0.022 (0.9) |-0.14 (0.34)|	0.067 (0.76) |0.22 (0.27)|	-0.084 (0.63) |0.16 (0.35)|	0.086 (0.61) |-0.15 (0.35)|	-0.1 (0.68) |0.36 (0.1)|	0.1 (0.68) |0.18 (0.44)|
Watershed Forested Area (%)	0.014 (0.94) |0.12 (0.45)|	0.058 (0.71) |-0.23 (0.12)|	-0.12 (0.42) |**-0.32 (0.03)**|	0.22 (0.27) |**0.53 (0.0033)**|	-0.063 (0.72) |-0.14 (0.42)|	-0.067 (0.7) |-0.13 (0.42)|	-0.23 (0.31) |0.23 (0.31)|	0.18 (0.44) |0.1 (0.68)|
Watershed Developed Area (%)	0.036 (0.83) |-0.065 (0.68)|	0.0072 (0.98) |0.25 (0.087)|	0.014 (0.94) |**0.38 (0.0082)**|	-0.37 (0.052) |**-0.48 (0.0086)**|	0.074 (0.68) |0.084 (0.63)|	0.019 (0.93) |0.1 (0.53)|	0.36 (0.1) |0 (1)|	-0.31 (0.16) |-0.026 (0.95)|
Watershed Planted Area (%)	0.039 (0.8) |-0.078 (0.61)|	0.093 (0.54) |**0.32 (0.036)**|	-0.031 (0.84) |0.18 (0.24)|	-0.27 (0.17) |**-0.45 (0.021)**|	0.17 (0.31) |0.17 (0.31)|	0 (1) |0.01 (0.95)|	0.27 (0.21) |-0.11 (0.61)|	-0.19 (0.38) |-0.055 (0.8)|
Average watershed slope	-0.1 (0.51) |0.029 (0.86)|	-0.058 (0.71) |**-0.35 (0.017)**|	0.065 (0.68) |-0.26 (0.078)|	0.32 (0.096) |0.33 (0.079)|	-0.053 (0.77) |-0.021 (0.92)|	0.0095 (0.98) |0.076 (0.65)|	-0.31 (0.16) |0 (1)|	0.21 (0.37) |0.077 (0.77)|
Average watershed elevation (masl)	-0.072 (0.64) |0.072 (0.64)|	-0.014 (0.94) |-0.19 (0.21)|	0.065 (0.68) |-0.13 (0.39)|	0.05 (0.82) |0.27 (0.17)|	0 (1) |-0.14 (0.42)|	0 (1) |-0.0095 (0.98)|	-0.051 (0.86) |0.051 (0.86)|	0.21 (0.37) |0.28 (0.2)|
WHR	**0.31 (0.034)** |0.036 (0.83)|	0.11 (0.48) |0.17 (0.27)|	-0.28 (0.062) |0.094 (0.54)|	-0.067 (0.76) |0.15 (0.45)|	-0.16 (0.35) |-0.23 (0.16)|	0.057 (0.74) |0.12 (0.46)|	-0.21 (0.37) |0.051 (0.86)|	0.21 (0.37) |-0.13 (0.59)|
Fr_{50}	0.072 (0.64) |-0.28 (0.062)|	0.014 (0.94) |0.029 (0.86)|	-0.065 (0.68) |-0.12 (0.45)|	0.2 (0.31) |-0.017 (0.96)|	-0.032 (0.87) |0.13 (0.46)|	0.22 (0.18) |0.25 (0.12)|	-0.26 (0.25) |-0.31 (0.16)|	**0.46 (0.03)** |-0.13 (0.59)|
NACW (m)	**0.31 (0.034)** |-0.0072 (0.98)|	0.065 (0.68) |0.14 (0.36)|	-0.28 (0.062) |0.18 (0.23)|	0.033 (0.89) |-0.15 (0.45)|	0.084 (0.63) |-0.18 (0.29)|	-0.14 (0.39) |0.19 (0.24)|	0.026 (0.95) |-0.13 (0.59)|	-0.18 (0.44) |-0.21 (0.37)|
Sinuosity (m/m)	**0.3 (0.039)** |0.16 (0.29)|	0.12 (0.45) |0.23 (0.12)|	**-0.31 (0.034)** |0.014 (0.94)|	-0.22 (0.27) |-0.067 (0.76)|	0.15 (0.39) |-0.053 (0.77)|	0.0095 (0.98) |0 (1)|	0.26 (0.25) |-0.051 (0.86)|	0 (1) |0.28 (0.2)|
$\frac{Q_{largest}}{Q_{2yr}}$	-0.14 (0.34) |-0.22 (0.14)|	-0.17 (0.25) |-0.1 (0.51)|	0.21 (0.16) |0 (1)|	-0.1 (0.63) |0.083 (0.69)|	-0.15 (0.39) |-0.011 (0.97)|	0.2 (0.22) |0.11 (0.49)|	-0.051 (0.86) |0.21 (0.37)|	-0.21 (0.37) |-0.28 (0.2)|

5. Discussion

5.1 Comparison with other studies

The average values of the exponents *b*, *f*, *m* obtained in this study are 0.230, 0.394 and 0.376, respectively, which are close to Lewis (1969) and Phillips & Scatena (2013) results in Puerto Rico (Fig. 3a), Leopold and Maddock's results in the Midwest US (Leopold & Maddock, 1953), and Leopold and Miller's results in ephemeral streams in US (Leopold & Miller, 1956). The *b* and *f* values agree with the prior work in Puerto Rico (Phillips & Scatena 2013) in that width (*b*) contributes a smaller component than depth (*f*) and velocity (*m*), and never exceeds one third (with only one minor exception; one site's value of *b* is 0.34). In 14 sites, velocity has the largest exponent, while depth has the largest exponent in the other 10 sites. Width never had the largest exponent, similar to Qin et al. (2020).

The ratio $\frac{f}{b}$ describes the shape of river banks (Ferguson, 1986), ranging from 0.93 to 12.89 in this study, with the median of 1.44. The majority of sites have ratios within or near the range 1-2, indicating that the majority of channel cross sections are either triangular or parabolic. The ratio at some sites, however, are higher, highlighting that there does exist a diversity of channel cross-sectional shapes in Puerto Rico including ones closer to rectangular.

The log-log linear relationship between the shape parameter $\frac{f}{b}$ and b are significant for both our data and a collection of parameters from former studies conducted in Puerto Rico, Colorado in the mountainous western United States, and the Yellow River in China. The fitted equations are all close to what Turowski et al. (2008) found using average values from other studies. Despite the strong log-log relationship between $\frac{f}{b}$ and b, we found that this relationship did not predict b as well as the regression-based model for that parameter (see Table 2; RMSE and rRMSE of b estimates based on the log-linear model are 0.61 and 265%). This may be due to the requisite log and exponential transformations. Nonetheless, the high similarity of the log-log linear relationship among different studies in highly varied geographic regions suggests the potential to estimate channel shape from the exponent b.

5.2 Hydraulic parameters and watershed and river reach characteristics

5.2.1 Exponents

The characteristics that were significantly correlated with the depth exponent f were inversely correlated with the velocity exponent m (Table 1), which is not unexpected due to the continuity requirement (Eqn. 4). These characteristics include upstream drainage area, the percentages of developed, forested and planted area, average upstream watershed slope and elevation. Our results are consistent with Klein (1981) and Qin et al. (2020), in that depth is a greater contributor for higher discharges in large rivers (positive correlation between watershed area and f), while width contributes more in small streams (negative—but not statistically significant—correlation between upstream watershed area and b). No watershed or river reach characteristics were found to be significantly (i.e. at the 5% level) correlated with the width exponent b.

Phillips and Scatena (2013) found that while velocity has a larger exponent for rural channels in Puerto Rico, depth contributes to a larger exponent extent in urban catchments. Our correlation results agree with this finding: the percentage of developed (forested) area of a watershed is positively (negatively) correlated with the depth exponent f and negatively (positively) with the velocity exponent m. This is further supported by the significant and positive correlation between $f - m$ and percentage of developed area (Kendall's tau = 0.54, p=10^{-4}). Cohesive banks are common in both developed and forested watersheds; with stable banks, the river channels have limited lateral adjustability (Millar and Quick, 1993; Millar, 2000). This potentially explains why land cover metrics were not significantly correlated with b. The positive correlation between f and the percentage of developed area indicates that the channels tend to adjust vertically in more developed watersheds than in more forested watersheds, which agrees with previous research showing that channels in urbanized environments are often prone to incision (Booth, 1990; Cole et al., 2017). In forested watersheds, wood load can contribute to flow resistance and is subject to adjustments from frequent and flashy floods (Cadol and Wohl, 2013), in support of the positive correlation between m (adjustability of channel roughness) and percent forested area.

The average elevation and slope of the watersheds are highly correlated (Kendall's tau=0.58; p<10^{-4}), and thus yield similar correlations with f (negative) and m (positive). Ran et al. (2012) and others have concluded that mountainous bedrock channels are typically stable, meaning scour and infill are negligible. This likely explains our result that higher-elevation and steeper (i.e. more mountainous) watersheds accommodate increasing discharge primarily through velocity (positive correlation with m) rather than depth (negative correlation with f).

5.2.2 Coefficients and bank shape parameters

Average watershed elevation was found to be negatively correlated with $\frac{f}{b}$ (Kendall's tau: -0.33, p=0.023; Table 4) and positively correlated with $\frac{c}{a^{\frac{f}{b}}}$. Since most channels have forms between triangular ($\frac{f}{b} = 1$) and parabolic ($\frac{f}{b} = 2$), this correlation suggests that lower-elevation channels tend to be parabolic with a gradually-sloped banks, while the higher-elevation channels tend to be triangular with steeper banks. This can be explained by the difference of channel substrate: higher-elevation watersheds are usually in mountainous areas with bedrock channels, while rivers in lower-elevation areas carry more alluvium which can be "shaped" into parabolic forms (Ran et al., 2012).

The coefficients in Eqns. 1-3 are unit-dependent, and are usually treated as values of width, depth or velocity when the discharge equals one unit (m^3/s in our case; Dingman & Afshari, 2018). The coefficients are general indicators of a channel's width, depth, and roughness. How these characteristics influence discharges at different flow levels is determined by exponents. For example, in Ran et al., 2012, a wide channel with highly-cohesive steep banks result in a high value of a and a relatively small value of b.

Upstream drainage area was significantly correlated with a (positive) and c (negative), and negatively but insignificantly correlated with k. This is similar to Qin et al. (2020), and suggests that channels in the larger watersheds in Puerto Rico are generally more "wide" than "deep," in terms of cross-sectional geometric controls on discharge. Reach width is significantly and positively correlated with a, confirming the interpretation of a as a scale factor for channel width (Ran et al., 2012). The significant positive correlation between reach width and k can be explained by continuity (Eqn. 4). Reach slope is found to be negatively significantly correlated with a, in support of that channels with greater slope have lower width to depth ratios due to less lateral adjustability of resistant bank material. The significant positive correlation between average watershed elevation and c shows that mountainous channels in Puerto Rico are usually deep, consistent with the observation mentioned above that channels at high elevations are more likely to be triangular rather than parabolic. High values of normalized active channel width reflect wide

channels relative to catchment size (by Eqn. 7; Morel et al., 2019), which could be indicative of increases in roughness associated with feedbacks between channel width and instream wood loading (negative correlation between normalized active channel width and k; Table 1), agreeing with former studies in that wood load increases flow resistance (Cadol & Wohl, 2013; Curran & Hession, 2013; McBride et al., 2007; McBride et al., 2008).

Coefficients are more influential when values of the variable (width, depth and velocity) are low, while exponents are more influential for high values. To demonstrate, we considered AHG parameters together with published flood stages obtained from National Weather Service (National Oceanic and Atmospheric Administration, 2021) to predict bankfull discharges based on Eqn. 2. We found that on average, exponents are more influential than coefficients at determining bankfull discharge at flood stage. For example, a 1% increase in f can resulted in an average decrease in bankfull discharge of 7.1%, while a 1% increase in c gave only an average decrease of 2.9%. It should be noted, however, that few sites have direct discharge measurements near or above these flood stages (see also Li et al. 2020 for discussion on this and other limitations in the PR field measurements), so these results should be taken with a grain of salt. This calls for further data to better understand the influence of both coefficients and exponents at flood discharges.

5.3 Predictive Models

The leave-one-out estimates reach an acceptable level of accuracy suggested by the relative RMSE. The root mean square errors (relative RMSEs) for estimates of b, f and m are 0.072 (31.16%), 0.073 (18.48%), and 0.060 (15.94%) [-], respectively. The RMSE and p-values are generally lower, and R-squared values generally higher, than Morel's models (Morel et al., 2019), likely due to a much reduced geographic scope and thus a smaller, more homogeneous set of sites. The RMSE (relative RMSE) for coefficients a, c and k are 3.3 s/m^2 (25.67%), 0.048 s/m^2 (18.26%) and 0.095 m^{-2} (28.18%), respectively. The high root mean square of a is due to its wide range and much higher magnitude compared to other parameters. The regression models not only yielded reliable estimates of the parameters at the study sites, but show the potential to predict parameter values for ungaged sites in similar environmental settings.

5.4 Tropical Cyclone Effects on AHG

The normalized two-year flood is positively correlated with real (i.e., not absolute) percent change of $\frac{c}{a^{\frac{f}{b}}}$, indicating that greater "flashiness" can steepen shapes after floods, possibly as a result of channel incision (e.g., Schumm et al. 1984; Simon & Rinaldi 2006; Wallerstein & Thorne, 2004). WHR is also positively correlated with real percent change of $\frac{c}{a^{\frac{f}{b}}}$, which shows that banks in channels with flatter cross-sections erode more readily than channels with steep banks, which is likely indicative of constraints on lateral adjustability imposed by consolidated or cohesive bank materials, or vegetative root reinforcement (Millar and Quick, 1993; Millar, 2000). Sinuosity, F_{50}, and NACW are positively correlated with the real percent change of a, showing that in meandering and wide channels and in channels with high F_{50}, channel widths tend to increase after floods. This is consistent with the expectation that sinuous channels are fully alluvial with laterally adjustable channel boundaries. The negative correlation between NACW and real percent change of k is probably caused by continuity requirement (Eqn. 4).

Average watershed slope is found to be negatively correlated with absolute percent change of c, consistent with the observation from section 5.2 that rivers in steeper watersheds are more stable. This agrees with former research that rivers in mountainous areas are usually supply limited and have resistant boundaries that are less responsive to changing in driving forces (Montgomery & Buffington, 1997; Montgomery & MacDonald, 2002). Reach width and watershed area are negatively correlated with absolute change of b, showing that channel width's contribution to discharge is relatively more (less) stable in the larger (smaller) study watersheds and wider (narrower) channels, agreeing with Qin et al. (2020) that river stability tends to increase with watershed area. The percentage of developed (forested) area is positively (negatively) correlated with the absolute change k, indicating that flow velocity is relatively more stable in forested watersheds than in urban channels facing TC floods. Flow velocities in locations with vegetated banks and large instream roughness elements tend to be confined to narrower ranges (Zong and Nepf, 2010; Curran & Hession, 2013), thus we would expect flow velocities to experience less change in forested areas than in more developed areas. The percentage of developed (forested) area is negatively (positively) correlated with the absolute change of b, showing that the lateral adjustability is more stable in developed watersheds than in forested ones. This makes sense since

urban channels are often anthropogenically confined. More data on channel boundary materials and vegetation could help future study analyze the stability of the river channels in Puerto Rico.

Li et al. (2020) found that river channels can experience both significant instant and gradual changes as responses to floods brought by TCs from a broader view focusing on channel conveyance capacity. How these conveyance capacity changes were achieved by river reaches, however, was not discussed in that paper. We herein elaborated on how channels adjust their geometry and roughness—changes of which can result in conveyance capacity changes—and identified potential predictors that render the channel geometry and roughness changes brought by TC floods more qualitatively predictable. Future studies on the quantitative connections between AHG parameter changes and conveyance capacity change are suggested; potentially applying AHG parameter regression models to conveyance capacity estimation. This could provide practical information for flood hazard management in dynamic channel networks.

6. Summary and Conclusions

River cross sectional geometry plays a critical role in fluvial processes (e.g. (Bennet & Bridge, 1995; Guan et al., 2016; Malkinson & Wittenberg, 2007). Power law at-a-station hydraulic geometry (AHG) formulations describing this geometry were introduced more than 60 years ago (Leopold & Maddock, 1953) and have been widely confirmed empirically and analyzed theoretically (e.g. (Andreadis et al., 2013; Barefoot et al., 2019; Dingman, 2007; Ferguson, 1986). The physical controls of AHG remain underexplored (Jia et al., 2017; Qin et al., 2020), however, especially in tropical areas which are generally less instrumented than more temperate zones.

In Puerto Rico, the intense precipitation brought by tropical cyclones (TCs) has been shown before to cause substantial changes to channel conveyance capacity via sediment redistribution (Li et al., 2020). That study failed to identify the mechanisms for such changes, however. In this study, we examine AHG at 24 stream gage sites in Puerto Rico, with a focus on understanding and modeling the upstream and river reach controls on AHG—with one goal being AHG estimation at ungaged sites—as well as how AHG can respond to major TC-induced floods. Key findings and conclusions are summarized here:

1. AHG parameters are highly correlated with a range of watershed and river reach characteristics; these relationships can largely be understood through existing geomorphological reasoning. AHG parameter estimates in this study are similar in magnitude to former studies in Puerto Rico.

2. AHG parameters can be robustly predicted using multiple linear regression with watershed and river reach characteristics. We can reach acceptable accuracy (relative RMSEs are usually between 10% and 30%) using these models, which could be used to predict AHG parameters in similar settings where cross sectional geometry data are lacking.

3. Some sites showed distinct changes in AHG—such as narrowed and deepened channels—after large floods, the large majority of which were caused by TCs. Certain watershed and river reach characteristics, specifically upstream watershed area, average watershed slope, watershed land cover, reach width, WHR, NACW, and sinuosity, are predictive both of whether and how AHG parameters change in response to floods.

Acknowledgments

Y. Li's contributions were supported by the Wisconsin Alumni Research Foundation.

Data Availability Statement

Field measurements, daily discharge records, site locations, and watershed shapefiles for all stream gaging sites available through U.S. Geological Survey NWIS system (U.S. Geological Survey, 2021a, 2021b). River network shapefile is available through U.S. Geological Survey, National Hydrography Dataset (U.S. Geological Survey, 2006). Percentages of developed area and forested area are available through the GAGES II data set (Falcone, 2011). The list of TCs that affected Puerto Rico during the study period is available through the HURDAT-2 data set (Landsea & Franklin, 2013). The digital elevation model is available through OCM Partners (2019). Codes used for analyses are available from the corresponding author.

References

Andreadis, K. M., Schumann, G. J.-P., & Pavelsky, T. (2013). A simple global river bankfull width and depth database: Data and Analysis Note. *Water Resources Research*, *49*(10), 7164–7168. https://doi.org/10.1002/wrcr.20440

Barber, C. A., & Gleason, C. J. (2018). Verifying the prevalence, properties, and congruent hydraulics of at-many-stations hydraulic geometry (AMHG) for rivers in the continental United States. *Journal of Hydrology*, *556*, 625–633. https://doi.org/10.1016/j.jhydrol.2017.11.038

Barefoot, E., Pavelsky, T. M., Allen, G. H., Zimmer, M. A., & McGlynn, B. L. (2019). Temporally Variable Stream Width and Surface Area Distributions in a Headwater Catchment. *Water Resources Research*, *55*(8), 7166–7181. https://doi.org/10.1029/2018WR023877

Bennet, S. J., & Bridge, J. S. (1995). The Geometry and Dynamics of Low-Relief Bed Forms in Heterogeneous Sediment in a Laboratory Channel, and their Relationship to Water Flow and Sediment Transport. *SEPM Journal of Sedimentary Research, Vol. 65A*. https://doi.org/10.1306/D4268013-2B26-11D7-8648000102C1865D

Best, H., McNamara, J. P., & Liberty, L. (2005). Association of Ice and River Channel Morphology Determined Using Ground-penetrating Radar in the Kuparuk River, Alaska. *Arctic, Antarctic, and Alpine Research*, *37*(2), 157–162. https://doi.org/10.1657/1523-0430(2005)037[0157:AOIARC]2.0.CO;2

Bridge, J. S. (1993). The interaction between channel geometry, water flow, sediment transport and deposition in braided rivers. *Geological Society, London, Special Publications*, *75*(1), 13–71. https://doi.org/10.1144/GSL.SP.1993.075.01.02

Brinkerhoff, C. B., Gleason, C. J., & Ostendorf, D. W. (2019). Reconciling at-a-Station and at-Many-Stations Hydraulic Geometry Through River-Wide Geomorphology. *Geophysical Research Letters*, *46*(16), 9637–9647. https://doi.org/10.1029/2019GL084529

Daly, C., Helmer, E. H., & Quiñones, M. (2003). Mapping the climate of Puerto Rico, Vieques and Culebra: CLIMATE MAPPING. *International Journal of Climatology*, *23*(11), 1359–1381. https://doi.org/10.1002/joc.937

David, G. C. L., Wohl, E., Yochum, S. E., & Bledsoe, B. P. (2010). Controls on at-a-station hydraulic geometry in steep headwater streams, Colorado, USA. *Earth Surface Processes and Landforms*, *35*(15), 1820–1837. https://doi.org/10.1002/esp.2023

Dingman, S. L. (2007). Analytical derivation of at-a-station hydraulic–geometry relations. *Journal of Hydrology*, *334*(1–2), 17–27. https://doi.org/10.1016/j.jhydrol.2006.09.021

Dingman, S. L., & Afshari, S. (2018). Field verification of analytical at-a-station hydraulic-geometry relations. *Journal of Hydrology*, *564*, 859–872. https://doi.org/10.1016/j.jhydrol.2018.07.020

Doll, B. A., Wise-Frederick, D. E., Buckner, C. M., Wilkerson, S. D., Harman, W. A., Smith, R. E., & Spooner, J. (2002). HYDRAULIC GEOMETRY RELATIONSHIPS FOR URBAN STREAMS THROUGHOUT THE PIEDMONT OF NORTH CAROLINA. *Journal of the American Water Resources Association*, *38*(3), 641–651. https://doi.org/10.1111/j.1752-1688.2002.tb00986.x

Falcone, J.A., 2011, GAGES-II: Geospatial Attributes of Gages for Evaluating Streamflow. Digital spatial data set, http://water.usgs.gov/GIS/metadata/usgswrd/XML/gagesII_Sept2011.xml.

Ferguson, R. I. (1986). Hydraulics and hydraulic geometry. *Progress in Physical Geography: Earth and Environment*, *10*(1), 1–31. https://doi.org/10.1177/030913338601000101

Fitzpatrick, F. A., & Knox, J. C. (2000). SPATIAL AND TEMPORAL SENSITIVITY OF HYDROGEOMORPHIC RESPONSE AND RECOVERY TO DEFORESTATION, AGRICULTURE, AND FLOODS. *Physical Geography*, *21*(2), 89–108. https://doi.org/10.1080/02723646.2000.10642701

Gleason, C. J. (2015). Hydraulic geometry of natural rivers: A review and future directions. *Progress in Physical Geography: Earth and Environment*, *39*(3), 337–360. https://doi.org/10.1177/0309133314567584

Gleason, C. J., & Smith, L. C. (2014). Toward global mapping of river discharge using satellite images and at-many-stations hydraulic geometry. *Proceedings of the National Academy of Sciences*, *111*(13), 4788–4791. https://doi.org/10.1073/pnas.1317606111

Guan, M., Carrivick, J. L., Wright, N. G., Sleigh, P. A., & Staines, K. E. H. (2016). Quantifying the combined effects of multiple extreme floods on river channel geometry and on flood hazards. *Journal of Hydrology*, *538*, 256–268. https://doi.org/10.1016/j.jhydrol.2016.04.004

Huang, Q., Long, D., Du, M., Zeng, C., Qiao, G., Li, X., Hou, A., & Hong, Y. (2018). Discharge estimation in high-mountain regions with improved methods using multisource remote sensing: A case study of the Upper Brahmaputra River. *Remote Sensing of Environment*, *219*, 115–134. https://doi.org/10.1016/j.rse.2018.10.008

Jia, Y., Yi, Y., Li, Z., Wang, Z., & Zheng, X. (2017). Integrating hydraulic equivalent sections into a hydraulic geometry study. *Journal of Hydrology*, *552*, 407–420. https://doi.org/10.1016/j.jhydrol.2017.06.039

Jowett, I. G. (1998). Hydraulic geometry of New Zealand rivers and its use as a preliminary method of habitat assessment. *Regulated Rivers: Research & Management: An International Journal Devoted to River Research and Management*, *14.5*, 451–466. https://doi.org/10.1002/(SICI)1099-1646(1998090)14:5<451::AID-RRR512>3.0.CO;2-1

Kale, V. S., & Hire, P. S. (2004). Effectiveness of monsoon floods on the Tapi River, India: Role of channel geometry and hydrologic regime. *Geomorphology*, *57*(3–4), 275–291. https://doi.org/10.1016/S0169-555X(03)00107-7

Kendall, M. G. (1938). A New Measure of Rank Correlation. *Biometrika*, *30*(1/2), 81. https://doi.org/10.2307/2332226

Klein, M. (1981). Drainage area and the variation of channel geometry downstream. *Earth Surface Processes and Landforms*, *6*(6), 589–593. https://doi.org/10.1002/esp.3290060608

Knighton, D., & Wharton. (2014). *Fluvial Forms and Processes: A New Perspective* (2nd ed.). Routledge. https://doi.org/10.4324/9780203784662

Landsea, C. W., & Franklin, J. L. (2013). Atlantic Hurricane Database Uncertainty and Presentation of a New Database Format. *Monthly Weather Review*, *141*(10), 3576–3592. https://doi.org/10.1175/MWR-D-12-00254.1

Lee, L., Lees, M., & Ridenour, G. S. (2019). Multi-Interval Data Mining of At-A-Station Hydraulic Geometry to Quantify Temporal Stability. *2019 IEEE 10th Annual Information Technology, Electronics and Mobile Communication Conference (IEMCON)*, 0501–0508. https://doi.org/10.1109/IEMCON.2019.8936151

Leopold, L. B., & Maddock, T. (1953). *The hydraulic geometry of stream channels and some physiographic implications* (Vol. 252). US Government Printing Office.

Leopold, L. B., & Miller, J. P. (1956). *Ephemeral streams—Hydraulic factors and their relation to the drainage net* (Vol. 282). US Government Printing Office.

Leopold, L. B., Wolman, M. G., & Miller, J. P. (1964). *Fluvial processes in geomorphology*. Freeman.

Lewis, L. A. (1969). SOME FLUVIAL GEOMORPHIC CHARACTERISTICS OF THE MANATI BASIN, PUERTO RICO. *Annals of the Association of American Geographers*, *59*(2), 280–293. https://doi.org/10.1111/j.1467-8306.1969.tb00671.x

Li, Y., Wright, D. B., & Byrne, P. K. (2020). The Influence of Tropical Cyclones on the Evolution of River Conveyance Capacity in Puerto Rico. *Water Resources Research*, *56*(9). https://doi.org/10.1029/2020WR027971

Malkinson, D., & Wittenberg, L. (2007). Scaling the effects of riparian vegetation on cross-sectional characteristics of ephemeral mountain streams—A case study of Nahal Oren, Mt. Carmel, Israel. *CATENA*, *69*(2), 103–110. https://doi.org/10.1016/j.catena.2006.04.026

Millar, R. G., & Quick, M. C. (1993). Effect of Bank Stability on Geometry of Gravel Rivers. *Journal of Hydraulic Engineering*, *119*(12), 1343–1363. https://doi.org/10.1061/(ASCE)0733-9429(1993)119:12(1343)

Montgomery, D. R., & Buffington, J. M. (1997). Channel-reach morphology in mountain drainage basins. *Geological Society of America Bulletin*, 16.

Montgomery, D. R., & MacDonald, L. H. (2002). DIAGNOSTIC APPROACH TO STREAM CHANNEL ASSESSMENT AND MONITORING. *Journal of the American Water Resources Association*, *38*(1), 1–16. https://doi.org/10.1111/j.1752-1688.2002.tb01530.x

675 Morel, M., Booker, D. J., Gob, F., & Lamouroux, N. (2020a). Intercontinental predictions of river hydraulic
676 geometry from catchment physical characteristics. *Journal of Hydrology*, *582*, 124292.
677 https://doi.org/10.1016/j.jhydrol.2019.124292
678 Morel, M., Booker, D. J., Gob, F., & Lamouroux, N. (2020b). Consistent Theoretical and Empirical
679 Predictions of at-a-Station Hydraulic Geometry Exponents in Stream Reaches. *Water Resources*
680 *Research*, *56*(10). https://doi.org/10.1029/2020WR027242
681 Morel, M., Tamisier, V., Pella, H., Booker, D. J., Navratil, O., Piégay, H., Gob, F., & Lamouroux, N. (2019).
682 Revisiting the drivers of at-a-station hydraulic geometry in stream reaches. *Geomorphology*, *328*,
683 44–56. https://doi.org/10.1016/j.geomorph.2018.12.007
684 National Oceanic and Atmospheric Administration. (2021). *National Weather Service*.
685 OCM Partners. (2019). 2016–2017 USGS Lidar DEM: Puerto Rico. *Charleston, SC: NOAA National*
686 *Centers for Environmental Information*. https://www.fisheries.noaa.gov/inport/item/55314
687 Ogden, F. L. (2016). Evidence of equilibrium peak runoff rates in steep tropical terrain on the island of
688 Dominica during Tropical Storm Erika, August 27, 2015. *Journal of Hydrology*, *542*, 35–46.
689 https://doi.org/10.1016/j.jhydrol.2016.08.041
690 Park, C. C. (1977). World-wide variations in hydraulic geometry exponents of stream channels: An analysis
691 and some observations. *Journal of Hydrology*, *33*(1–2), 133–146. https://doi.org/10.1016/0022-
692 1694(77)90103-2
693 Phillips, C. B., & Scatena, F. N. (2013). Reduced channel morphological response to urbanization in a
694 flood-dominated humid tropical environment: REDUCED CHANNEL MORPHOLOGICAL
695 RESPONSE TO URBANIZATION. *Earth Surface Processes and Landforms*, *38*(9), 970–982.
696 https://doi.org/10.1002/esp.3345
697 Qin, C., Wu, B., Wang, Y., Fu, X., Xue, Y., Li, D., Li, M., & Zhang, Y. (2020). Dynamic variability of at-
698 a-station hydraulic-geometry for mountain rivers in the southeast Qinghai-Tibet Plateau: The cases
699 of Yalong River and upper Jinsha River. *CATENA*, *194*, 104723.
700 https://doi.org/10.1016/j.catena.2020.104723

R core team. (2020). *R: A language and environment for statistical computing*. (4.0.3) [Computer software]. R Foundation for Statistical Computing. https://www.R-project.org/

Ran, L., Wang, S., & Lu, X. X. (2012). Hydraulic geometry change of a large river: A case study of the upper Yellow River. *Environmental Earth Sciences*, *66*(4), 1247–1257. https://doi.org/10.1007/s12665-011-1336-x

Reid, D. E., Hickin, E. J., & Babakaiff, S. C. (2010). Low-flow hydraulic geometry of small, steep mountain streams in southwest British Columbia. *Geomorphology*, *122*(1–2), 39–55. https://doi.org/10.1016/j.geomorph.2010.05.012

Reisenbüchler, M., Bui, M. D., Skublics, D., & Rutschmann, P. (2019). An integrated approach for investigating the correlation between floods and river morphology: A case study of the Saalach River, Germany. *Science of The Total Environment*, *647*, 814–826. https://doi.org/10.1016/j.scitotenv.2018.08.018

Shen, C., Wang, S., & Liu, X. (2016). Geomorphological significance of at-many-stations hydraulic geometry: Physical Interpretations of AMHG. *Geophysical Research Letters*, *43*(8), 3762–3770. https://doi.org/10.1002/2016GL068364

Slater, L. J., Singer, M. B., & Kirchner, J. W. (2015). Hydrologic versus geomorphic drivers of trends in flood hazard. *Geophysical Research Letters*, *42*(2), 370–376. https://doi.org/10.1002/2014GL062482

Smith, J. A., Sturdevant-Rees, P., Baeck, M. L., & Larsen, M. C. (2005). Tropical cyclones and the flood hydrology of Puerto Rico: TROPICAL CYCLONES AND FLOOD HYDROLOGY OF PUERTO RICO. *Water Resources Research*, *41*(6). https://doi.org/10.1029/2004WR003530

Stewardson, M. (2005). Hydraulic geometry of stream reaches. *Journal of Hydrology*, *306*(1–4), 97–111. https://doi.org/10.1016/j.jhydrol.2004.09.004

Su, T., Wang, S., Mei, Y., & Shao, W. (2015). Comparison of channel geometry changes in Inner Mongolian reach of the Yellow River before and after joint operation of large upstream reservoirs. *Journal of Geographical Sciences*, *25*(8), 930–942. https://doi.org/10.1007/s11442-015-1211-x

Turowski, J. M., Hovius, N., Wilson, A., & Horng, M.-J. (2008). Hydraulic geometry, river sediment and the definition of bedrock channels. *Geomorphology*, *99*(1–4), 26–38. https://doi.org/10.1016/j.geomorph.2007.10.001

U.S. Geological Survey. (2006). *National Hydrography Dataset (version 01_05)*. https://nhdplus.com/NHDPlus/ NHDPlusV1_21.php

U.S. Geological Survey. (2021a). *Peak Streamflow for the Nation*. https://nwis.waterdata.usgs.gov/usa/nwis/peak

U.S. Geological Survey. (2021b). *Streamflow Measurements for the Nation*. https://waterdata.usgs.gov/nwis/measurements

Wang, L., Sichangi, A. W., Zeng, T., Li, X., Hu, Z., & Genanu, M. (2019). New methods designed to estimate the daily discharges of rivers in the Tibetan Plateau. *Science Bulletin*, *64*(7), 418–421. https://doi.org/10.1016/j.scib.2019.03.015

Wang, S., Hassan, M. A., & Xie, X. (2006). Relationship between suspended sediment load, channel geometry and land area increment in the Yellow River Delta. *CATENA*, *65*(3), 302–314. https://doi.org/10.1016/j.catena.2006.01.003

West, A. J., Lin, C.-W., Lin, T.-C., Hilton, R. G., Liu, S.-H., Chang, C.-T., Lin, K.-C., Galy, A., Sparkes, R. B., & Hovius, N. (2011). Mobilization and transport of coarse woody debris to the oceans triggered by an extreme tropical storm. *Limnology and Oceanography*, *56*(1), 77–85. https://doi.org/10.4319/lo.2011.56.1.0077

Wiman, J., & Almstedt, A. E. (1997). Hydrodynamics, erosion and heat transfer in a pressurized fluidized bed: Influence of pressure, fluidization velocity, particle size and tube bank geometry. *Chemical Engineering Science*, *52*(16), 2677–2695. https://doi.org/10.1016/S0009-2509(97)00096-1

Yousefi, S., Mirzaee, S., Keesstra, S., Surian, N., Pourghasemi, H. R., Zakizadeh, H. R., & Tabibian, S. (2018). Effects of an extreme flood on river morphology (case study: Karoon River, Iran). *Geomorphology*, *304*, 30–39. https://doi.org/10.1016/j.geomorph.2017.12.034

Zhang, W., Wang, W., Zheng, J., Wang, H., Wang, G., & Zhang, J. (2015). Reconstruction of stage–discharge relationships and analysis of hydraulic geometry variations: The case study of the Pearl River Delta, China. *Global and Planetary Change*, *125*, 60–70. https://doi.org/10.1016/j.gloplacha.2014.12.004